

Morphological and microstructural characterization of $\text{Al}_{95}\text{Fe}_2\text{Cr}_2\text{Ti}_1$ powders produced by two different gas atomizers

Aylanna Priscila Marques de Araújo^{1,2,3*} 

Leandro Micheloti²

Claudio Shyinti Kiminami^{1,2}

Claudemiro Bolfari^{1,2}

Volker Uhlenwinkel³

Piter Gargarella^{1,2}

Abstract

This work aimed to produce powders of $\text{Al}_{95}\text{Fe}_2\text{Cr}_2\text{Ti}_1$ quasicrystalline phase former alloy using different atomizers, Hermiga (PH) and Spray forming/gas atomizer (PS), and investigate the powder characteristics as morphology, size distribution, flowability, microstructure, phase formation and thermal stability. The atomized powders were separated in different particles size ranges: $<32\mu\text{m}$, $32\text{-}45\mu\text{m}$ and $45\text{-}75\mu\text{m}$. The characterization of powder microstructure and morphology for each range was carried out by X-ray diffraction, Optical and Scanning Electron Microscopy, Differential Scanning Calorimetry (DSC) and semi-quantitative composition analysis by Energy Dispersive Spectrometer (EDS). The flowability was measured by Carney funnel. The PH powder presented a bimodal particle size distribution and its particles displayed a constant circularity and aspect ratio with microstructure rich in quasicrystalline phase. The PS powder showed a unimodal particle size distribution and the circularity and aspect ratio decrease with increasing particles size. The PS powder flowability was 1.6 times better than PH powder.

Keywords: Gas atomization; Rapid solidification; Al-based alloys; Physical and microstructural powder properties.

1 Introduction

Processes as gas atomization, spray deposition, splat quenching, melt spinning and planar flow casting impose high cooling rates during solidification and depending on the attained undercooling level their products can consist of different microstructures [1]. The gas atomization is an industrial rapid solidification process, which can produce large amounts of powder particles. As a consequence, this is the main commercial powder production method of aluminium and aluminium alloys. In the gas atomization method, a liquid stream of a molten alloy is disintegrated by high velocity gas, giving rise to spherical particles less than $200\mu\text{m}$ in diameter that solidify in a containerless way [2]. This process applies cooling rates around 10^5K/s [3], which are three orders magnitude higher than the cooling rate of water-cooled copper moulds [4]. Compared with water atomization the gas atomization achieves lower cooling rates although it produces more regular shape and uniform surface powders. However, different cooling rates can be achieved according to processing parameters as the gas-to-metal mass flow ratio (GMR), type and pressure of the atomization gas,

atmosphere in the atomization chamber and superheat. These parameters affect the particle size, morphology, satellite formation and surface texture of the powder particles [5]. Besides, even though particles more or less identical in size and shape from the same powder can show quite different microstructures because of different local conditions [1] the high solidification rate provides a refined structure and a more homogeneous chemical composition in the material [4].

Previous authors [6] investigated the influence of atomization gas pressure and melt mass flow on CuSn10 powders quality. They found that the circularity depends on the particle size so that larger particles show lower circularity. Others authors [7] studied the influence of atomizing gas pressure, delivery tube diameter and melt superheat on particle size and shape distribution of AlSi10Mg powders produced by double-nozzle gas atomization using different parameters. They detected that an increase of gas pressure and melt superheat or a decrease of the delivery tube diameter both led to a reduction of powder size, owing to the different melt mass flow rates and gas-to-metal ratio. Vlachos and

¹Programa de Pós-graduação em Ciência e Engenharia de Materiais – PPGCEM, Universidade Federal de São Carlos – UFSCar, São Carlos, SP, Brasil.

²Departamento de Engenharia de Materiais – DEMa, Universidade Federal de São Carlos – UFSCar, São Carlos, SP, Brasil.

³Universität Bremen, Leibniz Institut für Werkstofforientierte Technologien – IWT, Bremen, Germany.

*Corresponding author: aylannapriscula@hotmail.com



Chang [8] researched the relationship between flowability and powder physical properties (e.g. particle size and shape, size distribution and morphology). These authors observed that, despite research indicating that reduced powder size is associated with increased powder cohesion and, hence, poor flowability, adding controlled amounts of fine powders to a powder mixture doesn't necessarily reduce the flowability of the mixture. In addition, a change in flowability can be noticeable if particle size reduces at least ten times smaller than the biggest ones. Besides, elongated and irregular particles were found to have poor flowability [8]. Prior work [9] examined the shape and the satellite presence in the flowability of Fe-MnAlSi powders. They found a substantial improvement in flowability when powders were produced using an anti-satellite system [9].

Al-Fe-Cr-Ti alloys have been produced by gas atomization [2,10] aiming to obtain non-equilibrium microstructures. However, the biggest challenge is to produce a non-equilibrium and homogeneously dispersed microstructure. The mechanical strength of Al-Fe-Cr-Ti alloys can be improved when non-equilibrium microstructures, with refined grains, quasicrystalline phases and their approximants are homogeneously dispersed [11].

Nanometer-sized quasicrystalline phases with a homogeneous distribution in an α -Al solid solution matrix give rise to composites, which exhibit tensile yield strength around 600 MPa [12-14] at room temperature and if compared with amorphous aluminium alloys, they do not use expensive elements such as rare earths and zirconium. According to the literature [2,15] the atomized Al-Fe-Cr-Ti powder presented a microstructure of an aluminium matrix reinforced with a nanometer scaled, spherical quasicrystalline icosahedral phase. The quasicrystalline phase of the system Al-Fe-Cr-Ti transforms at about 500°C into the $Al_{13}Fe_4$, $Al_{13}Cr_2$ and Al_3Ti equilibrium phases [2]. Additionally, while the number and volume fraction of the quasicrystalline phases decrease as the powder particle size increases, the volume fraction of equilibrium phases increases [15].

So far, no systematic study has been carried out comparing properties of powders of an aluminium alloy prepared under different conditions, i.e. different atmospheres in the atomization chamber and gas atomization pressures. In addition, the formation of satellite particles in aluminium alloys depending on the different processing conditions has also not been investigated. It is expected that a large amount of satellite particles may decrease the flowability of powders as observed for other alloys [9], which may compromise its applicability in additive manufacturing and powder metallurgy.

Thus, the purpose of this study was to investigate the physical characteristics and microstructure of powders with the same chemical composition ($Al_{95}Fe_2Cr_2Ti_1$) and in the same particles size range ($< 75 \mu m$), which were produced using two different gas atomizers. They were produced in an atomizer with controlled atmosphere in the atomization chamber (under vacuum) and high atomization

pressure (named PH atomizer) and an atomizer with open atomization chamber and low atomization pressure (named PS atomizer). The properties of these two powders as particle size distribution, flowability, morphology and satellite formation, microstructure and thermal stability were evaluated and correlated with the atomization parameters used.

2 Materials and methods

Two ingots with composition of $Al_{95}Fe_2Cr_2Ti_1$ (%at.) were cast in an induction furnace available at the Casting Lab at DEMA/UFSCar using aluminium cans and pure elements (99.99% Al, 99.98% Fe, 99.99% Cr, 99.99% Ti). These ingots were atomized in two different equipments, PSI Hermiga 75/5VI gas atomizer and a spray forming/gas atomizer equipment produced by Gateway Engineering – England. The batches of powders were named PH and PS, respectively. The parameters used for each equipment are summarized in Table 1.

The gas-to-melt mass flow ratio (GMR) parameter is established as Equation 1 [6]:

$$GMR = \frac{M_g}{M_l} \quad (1)$$

where M_g and M_l means gas and metal mass, respectively.

A Malvern Mastersizer 2000 laser diffraction system with a water dispersion unit was used to measure the particle size distribution of the each batch of powders (PH and PS as atomized). The characteristic values measured are the mass median diameter $d_{50,3}$ and $d_{10,3}$, $d_{90,3}$ and the diameter ratio $d_{84,3}/d_{50,3}$. After that, each batch PH and PS was segregated in different size ranges ($75-45 \mu m$, $45-32 \mu m$ and $<32 \mu m$) by sieving.

To eliminate the effect of very small particles we chose the range $32-45 \mu m$ to measure the PH and PS powders flowability. The flowability measurements were carried out using Carney funnel (with orifice size of 5.0 mm) and 50 grams of powder. The procedure was based on ASTM B964 (method 2).

The microstructure of these powders was observed in a FEG Scanning Electron Microscopy (SEM) FEG XL-30 model and chemical analyses were performed by an

Table 1. Process parameters used during the gas atomizations for PH powder (PSI Hermiga 75/5VI gas atomizer) and PS powder (Gateway Engineering – England gas atomizer)

Parameters	PH	PS
Pouring temperature (°C)	870	725
Atomization pressure (bar)	40	10
Atomization gas	Ar	N ₂
Input mass (g)	2480	2590
Spray chamber atmosphere	Vacuum	Ambient
GMR	1.7	1.0

Energy Dispersive Spectrometer (EDS Oxford Instruments, X-act model) attached to the SEM. To evaluate the particles morphology the powders were analysed in a Malvern G3 optical measurement system. Since this is a particle imaging system, it is possible to quantify the circularity and aspect ratio of particles. The circularity parameter is determined by Equation 2 [6,16]:

$$C_i = 4\pi \frac{[Area]}{[Perimeter]^2} \quad (2)$$

where, C_i values closer to 1 mean a powder with more spherical shape particles. The phase formation was evaluated by X-ray Diffraction experiments (XRD) using a Siemens Model D5005 diffractometer with Cu-K α radiation, range 30-90° and step size of 2°/min. The thermal stability was investigated by Differential Scanning Calorimetry (DSC) using a Netzsch DSC 404 calorimeter with heating/cooling rate of 40 K/min and with argon protective atmosphere. Each particle size range was subjected to two heating cycles to evaluate the presence of quasicrystalline phases in the material.

3 Results and discussion

3.1 Morphological characterization

Prior to measuring flow properties of a collection of powders the size and morphology of particles should be known. Figures 1a, b display the volume density distribution and the accumulated mass distribution versus particle diameter for PH and PS powders as atomized. These curves are important to evaluate the distribution within a collection of particles and as commonly observed in gas atomized powders [10,15], the powders produced in this work showed a wide particle size range. As shown in Table 1, PH was produced under higher GMR and atomization pressure. According to Özbilen [5], high gas velocities in the jet and high gas pressure are

considered essential for the formation of a fine powder in the secondary breakup stage, both by ensuring a smaller critical size for the parent droplet at the end of disintegration and finer secondary breakup products. Thus, comparing PH and PS curves in Figures 1a, b, as expected, the cumulative distribution curves move to the left due to the increasing atomization pressure which means a reduction of powder size. Additionally, the GMR is important parameter that influence particle size and particle size distribution, where high GMR means more gas and higher gas velocities in the atomization zone and frequently provides smaller mean particles sizes [6]. As seen in the Figures 1a, b, the mass median diameter d_{50} is smaller for the PH powder (54.3 μm), which was produced under higher GMR, against 69.9 μm for PS powder. The PH curve of volume density distribution (Figure 1a) also presents a bimodal particle size distribution around 12 and 45 μm , whilst the PS curve presents a unimodal particle size distribution, with a diameter around 50 μm . Besides that, the diameter ratio $d_{84.3}/d_{50.3}$ is 1.69 for PH and 1.79 for PS. These results corroborates with the literature [5-7] and prove that PH powder, produced under higher gas pressure and GMR has a much smaller mean particle size than PS powder.

The morphological powders properties depend on the particles size, additionally, according to [5], the particles shape of gas atomised powder depends on the material being atomized. Table 2 summarizes the semi-quantitative measurements of the powder's chemical composition performed by EDS. It shows that their composition is very similar. All the measurements were treated statistically to obtain the average composition. Figures 2a-f show SEM images from different size ranges of the PH and PS powders. Since the morphology is driven by particles size, it indirectly depends on the GMR and gas pressure. Thus, comparing PH and PS for each corresponding range is possible to observe that, in the range <32 μm , PH powder (Figure 2a) shows a very large amount of small particles than PS powder (Figure 2b). The explanation is that PH was produced under higher gas pressure and GMR than PS

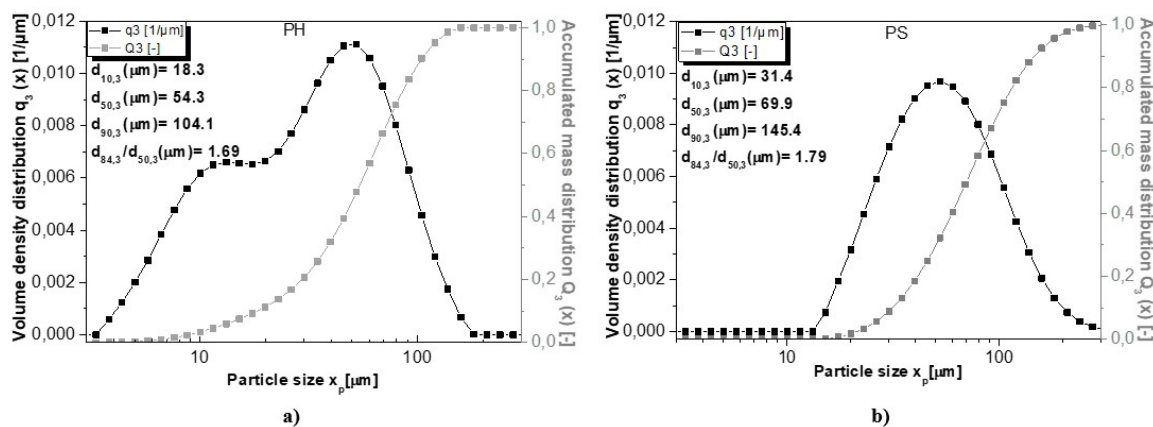


Figure 1. Volume density distribution and accumulated mass distribution as function of particle diameter for (a) PH and (b) PS powders.

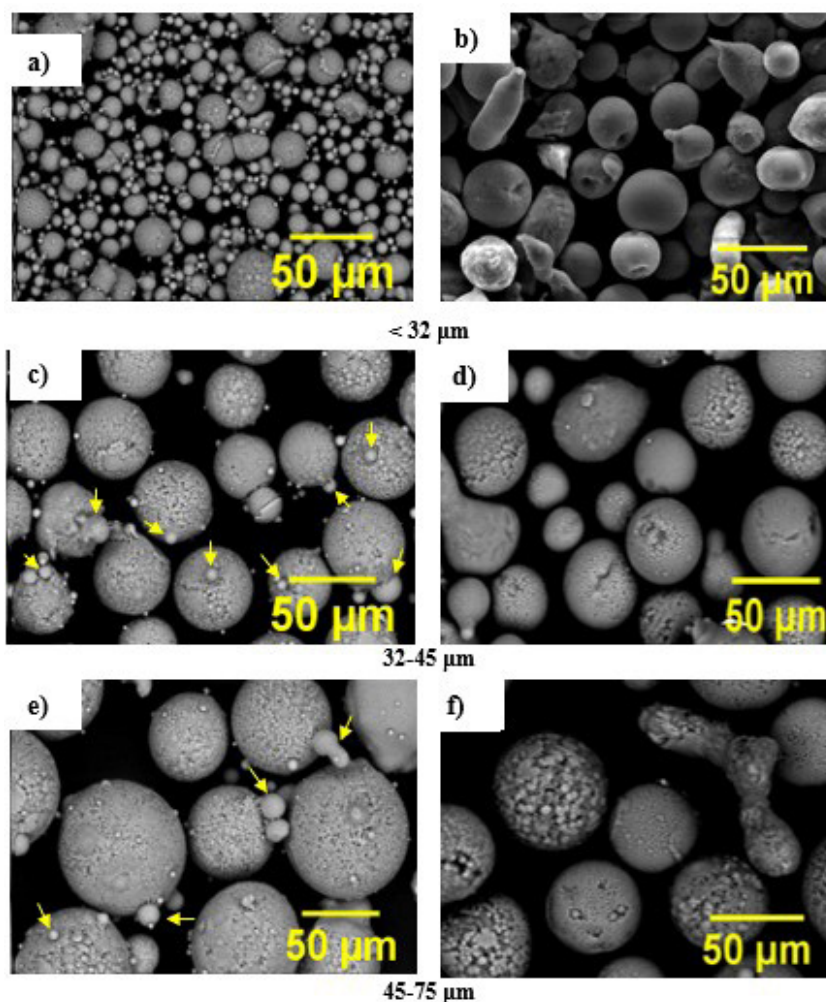


Figure 2. SEM (BSE mode) micrographs of PH (a), (c), (e) and PS (b), (d), (f) powders. The presence of satellites is indicated with yellow arrows.

Table 2. Chemical composition (%at.) for the PH and PS powders obtained by EDS

EDS	Al	Fe	Cr	Ti
PH powder	95.3±0.70	2.1±0.32	1.6±0.30	1.0±0.10
PS powder	95.0±1.49	2.5±0.77	1.8±0.46	0.8±0.14

powder. For ranges 32-45 μm (Figures 2c, d) and 45-75 μm (Figures 2e, f), even though the particles are in the same range, the PH powder particles are always more spherical and smoother than the PS powder particles. According to Özbilen [5] gas atomised powder particle shape and surface texture depend on the type of atomizing gas, the oxygen level and the operating pressure. The coarse powder becomes more irregular in shape and rougher on the surface when atomisation is carried out under oxidising conditions [5]. This occurs due to inhomogeneous surface oxide film thickness. In this work, as shown in Table 1, the PH atomized using argon gas and spray chamber under vacuum (low oxygen level) in combination with gas pressure of 40 bar resulted in well round and smooth particles, while the PS powder, produced using nitrogen gas (N_2) and spray chamber under

ambient atmosphere (high oxygen level) in combination with gas pressure of 10 bar resulted in irregular particles and rough surface texture.

The powder particles sphericity can be measured by circularity (Equation 2) and aspect ratio parameters. These are important powder parameters to quantify morphologically a group of powder particles. The values of circularity and aspect ratio for PH and PS powders for each size range are summarized in Figure 3. The PH curves show a constant circularity and aspect ratio with the increasing particle size range. On the other side, the PS curves show a decrease of these characteristics with increasing particles size range. These results are in agreement with SEM results and are a consequence, as mentioned before, of two different combinations of atomization parameters.

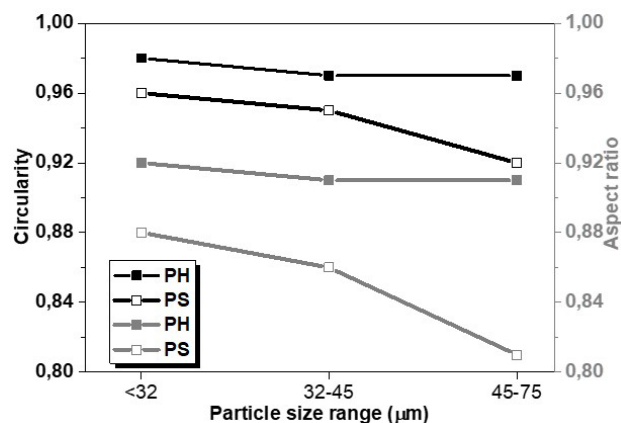


Figure 3. Circularity and aspect ratio of the PH and PS powders analysed by Malvern G3.

Morphological particles characteristics as circularity, aspect ratio and texture surface are important parameters for the capacity of powders transport (flowability). Also, it is known that flowability depends on the particle size powder. According to Vlachos and Chang [8], despite researches indicating that reduced powder size is associated with increased powder cohesion and, hence, poor flowability, adding controlled amounts of fine powders to a powder mixture doesn't necessarily reduce the flowability of the mixture. In this work, to reduce the effect of the really small particles presents in PH powder (<32 µm) and the strong irregularity of the big particles in PS powder (45-75 µm), it was selected the 32-45 µm particle size range to investigate the flowability. The PH powder presented 0.3 ± 0.04 g/s of flowability, whilst the PS powder 0.5 ± 0.1 g/s, which suggest that the PH has worst flowability than the PS powder. According to literature [8], the flow rate increases with increasing aspect ratio and circularity. Since irregular shape can influence particle-particle friction and cause physical interlocking during flowing, restricting the slippage required for flow [8]. Therefore, although it has been expected better flowability for PH powder due to its higher circularity, aspect ratio and smoother particle surface, as was observed by SEM, the PS powders showed a better capacity to flow. The poor flowability of the PH powder must be mainly attributed to the satellite particles presence. In spite of the constant circularity and aspect ratio for PH when compared different size ranges, as showed in Figure 3, is important to point out the presence of satellites in this powder, mainly in the 32-45 µm range. Satellite particles result of the existence of smaller particles firmly attached by welding to larger ones during fly [5]. The formation of satellites requires a number of large particles on to which relatively smaller particles (candidate for satellite formation) which not only collides with the larger ones (as a result of velocity differences arising from mass differences of coarse and fine particles), also firmly attach to them. In this study, satellite formation was observed only in the form of very small particles (typically <5 µm) attached to much larger ones (Figures 2c, e) but not between particles of

comparable size (Figure 2a). According to Özbilen [5], this behavior suggests that a differential acceleration in flight is an important cause of satellite formation. Considering that small particles present a higher acceleration and have higher velocities at a given position below the nozzle than large ones, welding of particles would take place as a result of the impact, even when the large particle is fully solidified [5]. When the large particle is a liquid droplet above the melting point, the satellite may in principle dissolve or embedding may occur, depending on the actual conditions of impact and heat transfer obtained. This would also apply when the large particle is liquid but undercooled, in which case the result is likely to be an embedded satellite.

As shown in Figures 2a, c, e the PH powder particles present a quite spherical morphology but with much more satellites than PS powder (Figures 2b, d, f). Also as confirmed by examining PH particles with size < 32 µm (Figure 2a) few satellites and abundant fine particles (not satellites) are present. On the other side, the PS powder showed particles more elongated and irregular, without presence of satellites, which resulted in a better flowability.

Taking into the results so far, powders with the same composition and similar particle size range, produced by different equipments, do not have the same qualities in terms of morphological and physical properties. As a consequence, the flowability behavior and processability in powder metallurgy and additive manufacturing processes can be strongly impacted.

3.2 Microstructural characterization

As reported in literature [3], cooling rate in molten metal gas atomization is the key determining factor for the microstructure of metal powders [3]. Figures 4a, b show the XRD patterns of the PH and PS powders with particle size <32 µm, 32-45 µm and 45-75 µm. The powders microstructure consists of $\alpha\text{-Al}$, $\text{Al}_{13}(\text{Cr,Fe})_{2,4}$, quasicrystalline phase (QC phase) and $\text{Al}_{13}\text{Cr}_2$. The peaks that correspond to the QC phase and/or $\text{Al}_{13}(\text{Cr,Fe})_{2,4}$ are observed for both powders. As $\text{Al}_{13}(\text{Cr,Fe})_{2,4}$ and $\text{Al}_{13}\text{Cr}_2$ are QC approximant phases, an overlapping of strong peaks corresponding to the QC phase and metastable $\text{Al}_{13}(\text{Cr,Fe})_{2,4}$ and/or stable $\text{Al}_{13}\text{Cr}_2$ phases can occur. The main QC phase peak in PH powder ($\sim 43^\circ$) seems to split in two others peaks (Figure 4a marked by arrows) with increasing the particle size. On the other side, for PS powder the peak relative to the QC phase (Figure 4b) moves slightly to higher angles with increase the particles size. These alterations can be explained due to the presence of phases similar to the QC phase as $\text{Al}_{13}(\text{Cr,Fe})_{2,4}$ and/or $\text{Al}_{13}\text{Cr}_2$.

According to [2] the smaller the particle size the higher the cooling rate. As the QC phase is metastable, is expected the number and volume fraction of the QC phase decrease, while the volume fraction of equilibrium phases increases as the powder particle size increases. Besides, the PS powder diffractograms evidenced the formation of Al_3Ti_1 or

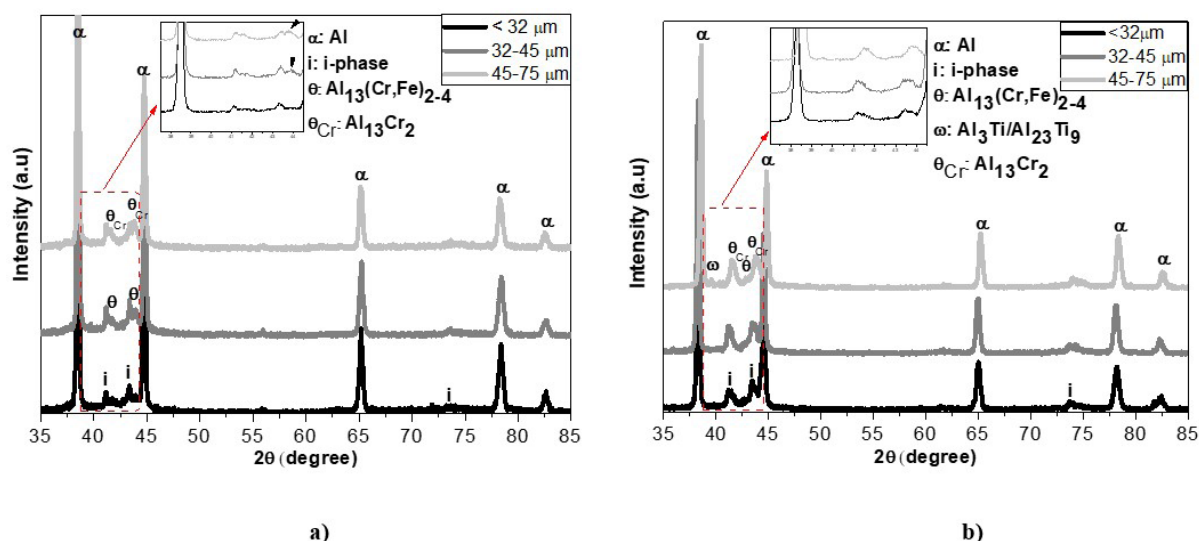


Figure 4. X-ray diffractograms of the (a) PH and (b) PS powders.

$\text{Al}_{23}\text{Ti}_9$ phase for the size range 45–75 μm (bigger size range). The precipitation of the $\text{Al}_3\text{Ti}_1/\text{Al}_{23}\text{Ti}_9$ compound tends to increase with decreasing cooling rate [17]. According to [3] in addition to the droplet diameter, the GMR has a strong influence on the cooling rate with higher GMR resulting in higher cooling rates. Thus, the PS powder produced using lower GMR (GMR = 1.0) provided lower cooling rates, which allowed the formation of the $\text{Al}_3\text{Ti}_1/\text{Al}_{23}\text{Ti}_9$ phase. The formation of these phases was also observed in previous works with Al-Fe-Cr-Ti alloys [17–21].

As reported by Ciftci et al. [3] the particle size alters the cooling rates and a higher GMR leads to higher cooling rates up to particle sizes of 45 μm . In this work, aiming to investigate the effect of GMR on the powder's microstructure the size range of 32–45 μm for both powders (PH and PS) was analyzed by SEM. Figures 5a–f show the microstructure of the PH and PS powders in the same size range (32–45 μm). Figure 5a shows particles with similar size but different microstructures: while one is very rich in QC phase (Figure 5b) the other is almost free of such phase. The phase formation and microstructure are strictly related to the cooling rate and to local solidification conditions. It is important to point out that smaller particles tend to cool more rapidly and/or undercool more prior to solidification and this condition promotes higher solidification rates [2,3]. However, similar particles in size and shape from the same powder sample can sometimes present quite different solidification conditions [1].

An extensive survey of many BSE SEM images from the PH and PS powders samples leads to the conclusion that there are α -Al matrix and QC phase for both powders yet a higher amount of QC phase is observed for PH powder. Examples of BSE SEM images from each powder are shown in Figure 5. According to the literature [18,21,22] the QC phase can be recognized by its features as morphology and size. The QC phase morphology observed in this

work is quite similar to the spherical QC phase observed in [23]. The QC phase is indicated in Figures 5b, d by dashed circles, presenting spherical morphology and its measured chemical composition is shown in the images. The PS powder microstructure also presents a metastable $\text{Al}_{13}(\text{Cr,Fe})_{2,4}$ phase (filled circle in Figure 5c) and a small amount of intermetallic phases as $\text{Al}_{13}\text{Fe}_4$ and Al_3Ti_1 in the interdendritic areas. The $\text{Al}_{13}(\text{Cr,Fe})_{2,4}$ phase can be recognized as a phase precedent of the flower-like phase. This phase is rich in chromium and iron as proved by EDS and is well-known as an approximant of the QC phase common in Al-Cr-Fe-X alloys [24–27]. These results suggest that most of the PH powder particles (GMR= 1.7) underwent cooling rates enough to form a high amount of QC phase, whilst the most of the PS powder (GMR = 1.0) underwent cooling rate that provided a longer solidification time with the formation of intermetallic phases as $\text{Al}_3\text{Ti}_1/\text{Al}_{23}\text{Ti}_9$ phase. The powders microstructural results are supported by the XRD diffractograms and agree with the literature [2].

Solid-state phase transformations were investigated by DSC for each powder size ranges in order to confirm the presence of QC phase. The DSC results are given in Figure 6a, b. The PH powders curves show an exothermic event at $\sim 550^\circ\text{C}$, which correspond to the phase transformation of the QC and/or $\text{Al}_{13}(\text{Cr,Fe})_{2,4}$ phases into the $\text{Al}_{13}\text{Fe}_4$, $\text{Al}_{13}\text{Cr}_2$ and Al_3Ti equilibrium phases. The exothermic events related to the QC decomposition observed in this work are similar to those obtained in previous works dealing with gas-atomized powder and spray-formed ingots of other similar Al-Fe-Cr-Ti alloys [28–30]. The heat released in this reaction decreased with increasing the particle size, being higher for the PH powder with smaller particle size (< 32 μm) than 32–45 μm and 45–75 μm (Figure 6a). As mentioned before the QC phases decrease in number and volume fraction as the powder particle size increases [15]. For PS powder this exothermic event was only detected in the range of <32 μm

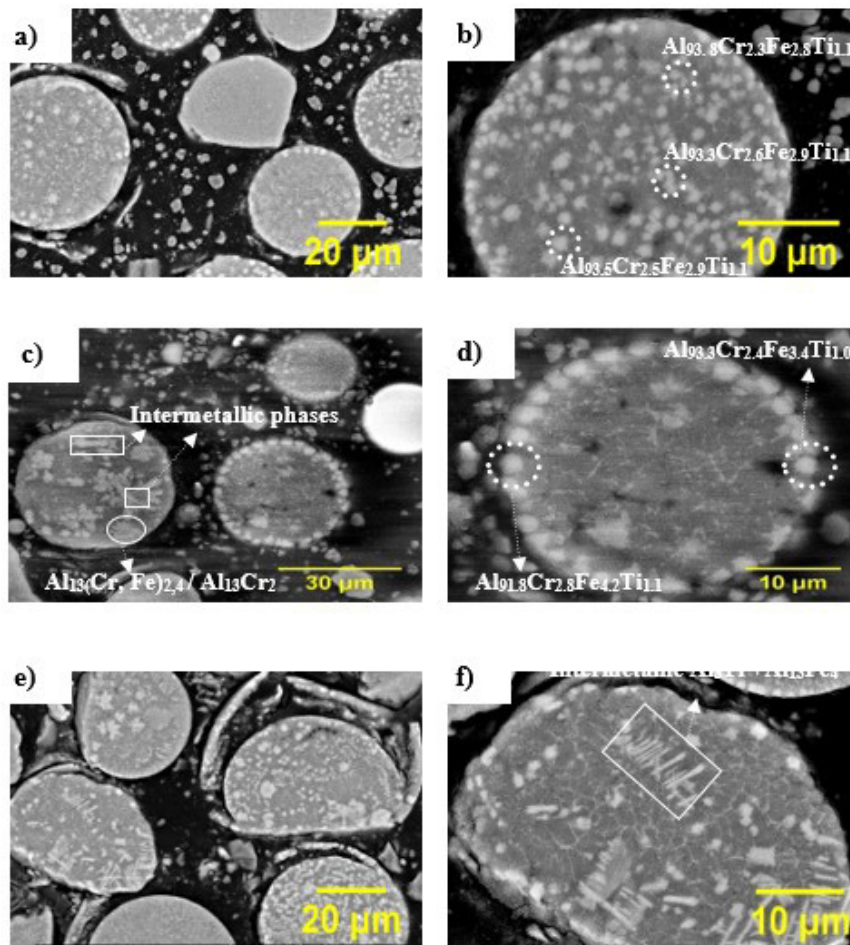


Figure 5. SEM (BSE mode) micrographs of (a), (b) PH and (c), (d), (e), (f) PS powders with granulometry in the range 32-45 μm .

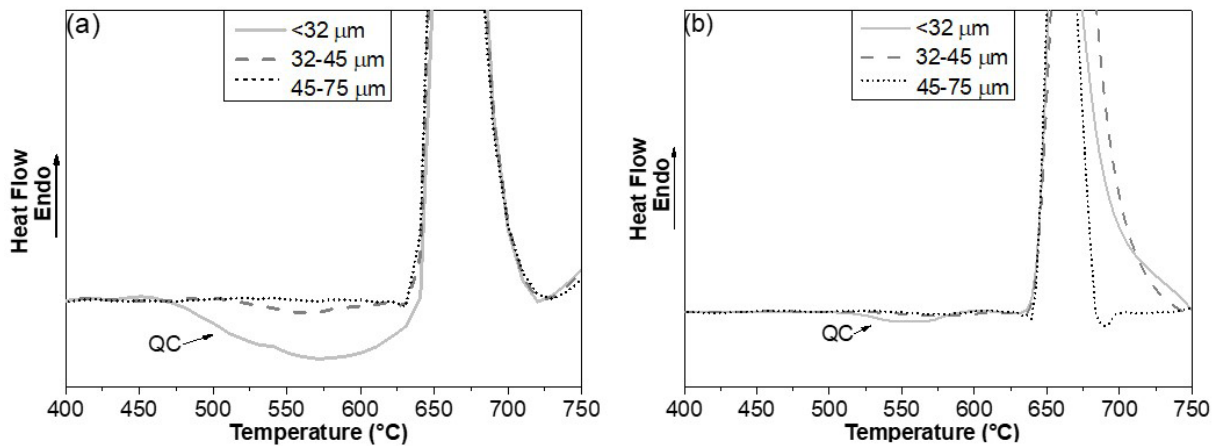


Figure 6. DSC thermal analysis of (a) PH and (b) PS powders.

(Figure 6b). As expected, larger particles underwent lower cooling rates and formed lower amount of QC phase, and as a result, the exothermic peak is not evident for size ranges greater than 45 μm for PH powder and greater than 32 μm for PS powder. The DSC traces are in agreement with XRD and SEM images results.

4 Conclusions

When compared the physical characteristics and microstructural of powders with the same chemical composition ($Al_{95}Fe_2Cr_2Ti_1$) and in the same particles size range (< 75 μm), which were produced using two different

atomizers, were obtained that: 1) powders with same composition and similar particle size range, produced by different equipments, do not have the same qualities in terms of morphological, physical and microstructural properties; 2) the PH powder produced under GMR=1.7 and 40 bar of atomization pressure, presented a larger amount of powder in the range <32 μm ; 3) the PH powder produced using argon gas and controlled vacuum condition during atomization exhibited more spherical particles with quite smooth surface; 4) in the range 32–45 μm the PH powder presented a higher amount of satellite particles attached on bigger particles; 5) while circularity and aspect ratio of the PH powder are constant for the different particles size ranges, the circularity of PS powder decreases with increasing particle size; 6) the circularity and aspect ratio of PH powder measured by G3 were not affected by the presence of satellite particles; 7) even though the PH powder presented morphological properties beneficial for good flowability (i.e. particles

well spherical and smooth surface) the PS powder showed flowability 1.6 times better by Carney funnel. This difference was attributed mainly to the presence of satellite particles in the PH powder; 8) the PH powder microstructure for the particles size range <32 μm showed an α -Al matrix richer in QC phase than PS powder in the same range; 9) DSC curves traces showed the presence of QC phase in the PH powders with size below 45 μm and the PS powder with size below 32 μm . Smaller particle sizes resulted in a larger volume of QC phase, with a larger exothermic transformation peak.

Acknowledgements

FAPESP projects n°. 2017/27031-4, n°. 2016/11309-0 and n°. 2018/04209-5. CNPq project n°. 400834/2016-2. This study was financed in part by the Coordenação de Aperfeiçoamento de Pessoal de Nível Superior - Brasil (CAPES) - Finance Code 001.

References

- 1 Suryanarayana C. Non-equilibrium processing of materials. 1st ed. Amsterdam: Elsevier; 1999.
- 2 García-Escorial A, Lieblich M. Atomization of Al-rich alloys: three paradigmatic case studies. *Journal of Alloys and Compounds*. 2018;762:203-208.
- 3 Ciftci N, Ellendt N, Coulthard G, Barreto ES, Mädler L, Uhlenwinkel V. Novel cooling rate correlations in molten metal gas atomization. *Metall and Materi Trans B*. 2019;50:666-677.
- 4 Yefimov NA. Powders with quasicrystalline structure. In: Neikov OD, Naboychenko SS, Yefimov NA. *Handbook of non-ferrous metal powders*. Amsterdam: Elsevier; 2019 [cited 2019 June 21]. Available at: <https://linkinghub.elsevier.com/retrieve/pii/B9780081005439000105>
- 5 Özbilen S. Satellite formation mechanism in gas atomised powders. *Powder Metallurgy*. 1999;42:70-78.
- 6 Schwenck D, Ellendt N, Fischer-Bühner J, Hofmann P, Mädler L, Uhlenwinkel V. Effect of Process Parameters on Powder Quality. In: SDMA. 5th Int Conf on Spray Deposition and Melt Atomization. Bremen, Germany; Bremen: SDMA; 2013. p. 12.
- 7 Gao C, Xiao Z, Zou H, Liu Z, Chen J, Li S, et al. Characterization of spherical AlSi10Mg powder produced by double-nozzle gas atomization using different parameters. *Transactions of Nonferrous Metals Society of China*. 2019;29:374-384.
- 8 Vlachos N, Chang ITH. Investigation of flow properties of metal powders from narrow particle size distribution to polydisperse mixtures through an improved Hall-flowmeter. *Powder Technology*. 2011;205:71-80.
- 9 Mostaghimi F, Fischer-Bühner J, Heemann L, Hofmann P, von Hehl A, Uhlenwinkel V. Anti-satellite system for the improvement of powder quality in additive manufacturing using a FeMnAlSi alloy. In: *European Powder Metallurgy Association. Proceedings of the Euro PM2018*. Bilbao, Spain; Bilbao: EPMA; 2018.
- 10 Dám K, Vojtěch D, Průša F. Powder metallurgy Al–6Cr–2Fe–1Ti alloy prepared by melt atomisation and hot ultra-high pressure compaction. *Materials Science and Engineering A*. 2013;560:705-710.
- 11 Inoue A, Kimura H. High-strength aluminum alloys containing nanoquasicrystalline particles. *Materials Science and Engineering A*. 2000;286:1-10.
- 12 Inoue A, Kimura H, Sasamori K, Masumoto T. High mechanical strength of Al–(V, Cr, Mn)–(Fe, Co, Ni) quasicrystalline alloys prepared by rapid solidification. *Materials Transactions*. 1996;37:1287-1292.
- 13 Inoue A, Kimura H, Yamaura S. Production and mechanical properties of aluminum alloys with dispersed nanoscale quasicrystalline and amorphous particles. *Metals and Materials International*. 2003;9:527-536.
- 14 Galano M, Audebert F, Escorial AG, Stone IC, Cantor B. Nanoquasicrystalline Al–Fe–Cr-based alloys. Part II. Mechanical properties. *Acta Materialia*. 2009;57:5120-5130.

- 15 Bártová B, Vojtěch D, Verner J, Gemperle A, Studnička V. Structure and properties of rapidly solidified Al–Cr–Fe–Ti–Si powder alloys. *Journal of Alloys and Compounds*. 2005;387:193-200.
- 16 Cui C, Uhlenwinkel V, Schulz A, Zoch H-W. Austenitic stainless steel powders with increased nitrogen content for laser additive manufacturing. *Metals*. 2019;10:61.
- 17 Garcia-Escorial A, Natale E, Cremaschi VJ, Todd I, Liebllich M. Quasicrystalline Al₉₃Fe₃Cr₂Ti₂ alloys. *Revista de Metalurgia*. 2015;51(4):e054.
- 18 Galano M, Audebert F, Stone IC, Cantor B. Nanoquasicrystalline Al–Fe–Cr-based alloys. Part I: Phase transformations. *Acta Materialia*. 2009;57:5107-5119.
- 19 Galano M, Audebert F, Escorial AG, Stone IC, Cantor B. Nanoquasicrystalline Al–Fe–Cr-based alloys with high strength at elevated temperature. *Journal of Alloys and Compounds*. 2010;495:372-376.
- 20 Yamasaki M, Nagaishi Y, Kawamura Y. Inhibition of Al grain coarsening by quasicrystalline icosahedral phase in the rapidly solidified powder metallurgy Al–Fe–Ti–Cr alloy. *Scripta Materialia*. 2007;56:785-788.
- 21 Inoue A, Kimura H. High elevated-temperature strength of Al-based nanoquasicrystalline alloys. *Nanostructured Materials*. 1999;11:221-231.
- 22 Kang N, Fu Y, Coddet P, Guelorget B, Liao H, Coddet C. On the microstructure, hardness and wear behavior of Al-Fe-Cr quasicrystal reinforced Al matrix composite prepared by selective laser melting. *Materials & Design*. 2017;132:105-111.
- 23 Leonard HR. Development of quasicrystal morphology in gas-atomized icosahedral-phase-strengthened aluminum alloy powders. *Materials & Design*. 2019;182:10.
- 24 Audebert F, Galano M, Rios CT, Kasama H, Peres M, Kiminami C, et al. Nanoquasicrystalline Al–Fe–Cr–Nb alloys produced by powder metallurgy. *Journal of Alloys and Compounds*. 2013;577:650-657.
- 25 Galano M, Audebert F, Cantor B, Stone I. Structural characterisation and stability of new nanoquasicrystalline Al-based alloys. *Materials Science and Engineering A*. 2004;375–377:1206-1211.
- 26 Stan-Głowińska K. Formation of Quasicrystalline Phases and Their Close Approximants in Cast Al-Mn base alloys modified by transition metals. *Crystals*. 2018;8:61.
- 27 Khoruzha VG, Kornienko KE, Pavlyuchkov DV, Grushko B, Velikanova TY. The Al–Cr–Fe phase diagram. I. Phase equilibria at subsolidus temperatures over composition range 58–100 at.% Al. *Powder Metallurgy and Metal Ceramics*. 2011;50:83-97.
- 28 Garcia-Escorial A, Echevarria M, Liebllich M, Stone I. Characterisation of an Al₉₃Fe₃Cr₂Ti₂ alloy obtained by spray forming. *Journal of Alloys and Compounds*. 2010;504:S519-S521.
- 29 García-Escorial A, Natale E, Cremaschi VJ, Todd I, Liebllich M. Microstructural transformation of quasicrystalline AlFeCrTi extruded bars upon long thermal treatments. *Journal of Alloys and Compounds*. 2015;643:S199-S203.
- 30 Todd I, Chlup Z, O'Dwyer JG, Liebllich M, García-Escorial A. The influence of processing variables on the structure and mechanical properties of nano-quasicrystalline reinforced aluminium alloys. *Materials Science and Engineering A*. 2004;375–377:1235-1238.

Received: 02 Abr. 2020

Accepted: 07 Mai. 2021